Characterizations of MnO_2 doped TiO_2 nanostructures and effective degradation of methylene blue dye under visible light irradition

R. Thambidurai[a], G. Gobi[a,*], R. Uthrakumar[a], C. Inmozhi[b], K. Kaviyarasu[c,d]
[a]*Department of Physics, Govt. Arts College (Autonomous), Salem - 636007, Tamil Nadu, India*
[b]*Department of Physics, Govt. Arts College for Women, Salem - 636008, Tamil Nadu, India*
[c]*UNESCO-UNISA Africa Chair in Nanosciences/Nanotechnology Laboratories, College of Graduate Studies, University of South Africa (UNISA), Muckleneuk Ridge, PO Box 392, Pretoria, South Africa*
[d]*Nanosciences African Network (NANOAFNET), Materials Research Group (MRG), iThemba LABS-National Research Foundation (NRF), 1 Old Faure Road, 7129, PO Box 722, Somerset West, Western Cape Province, South Africa*

Pure and TiO_2 doped MnO_2 nanoparticles were made using a simple sol-gel technique, and their structural, morphological, characteristics were characteristically examined using XRD, FTIR, and UV-Visible and photocatalytic analysis. Through XRD and SEM analyses, a tetragonal crystalline structure with spherical nanoparticles was discovered. The EDAX experiments provide additional evidence of TiO_2's presence in the MnO_2 crystal matrix. From UV spectral studies, the band gap energy of MnO_2 doped was determined. Photo-degradation study was monitored using methylene blue (MB) and phenol dye solution under visible light irradiation. MnO_2 doped catalyst displayed exceptional photocatalytic efficacy towards MB dye under ideal conditions.

(Received April 6, 2023; Accepted July 21, 2023)

Keywords: MnO_2 doped TiO_2, Sol-gel, Photo-degradation, Methyl orange, Visible light, Electron-hole separation

1. Introduction

Natural substances are known as water poisons, and they appear in various forms in the food, clothing, leather, medicinal, and plastic industries [1, 2]. Due to their semi-volatility, greater water dissolvability, high lipid solvency, persistence, and high atomic weight, these natural pollutants are harmful to the ecosystem, dangerous to human health, and challenging to degrade. Large-scale treatment methods, such as photochemical degradation, natural debasement, chemical oxidation, ultrasound debasement, coagulation and flocculation, Advanced Oxidation Process (AOPs), and adsorption, have subsequently been tested for the expulsion of dyes from natural waters and wastewater sources [3–9]. Photocatalyst is an excellent approach for separating organic pollutants from other types of pollutants in the atmosphere. The removal of pollutants from the environment and the development of self-cleaning glass are just a few of the astounding practical uses of photocatalysis, which is a crucial component of research in the field. Due to their narrow band gap, tunable electronic configuration, desired physico-chemical properties, and high absorption capacity [14–16], semiconducting based metal oxides such as TiO_2 [10], WO_3 [11], ZnO [12], and SnO_2 [13] catalyst is generally very effective material. Manganese oxide (MnO2) has drawn the most interest among these due to its favourable environmental effects, high reversibility, and greater economic value [14-16]. In the presence of a catalyst, it can also be readily adjusted to the right physical and chemical properties. The visible light has been readily absorbed due to the appropriate band gap energy (2.6 eV), which is more beneficial for photo-

* Corresponding author: gobi.rect@gmail.com
https://doi.org/10.15251/DJNB.2023.183.869

degradation performance due to the better electronic conducting nature. Various areas, including those involving super capacitors, batteries, sensors, optoelectronic devices, and catalytic applications, have made extensive use of MnO_2 [17–19]. According to Zhang et al. [20], the methylene blue decomposition of MnO_2 nanorods is highly effective. High degradation efficiency of various toxic pollutants using the MnO2 catalyst was reported by Sui et al. [21]. MnO_2 nanopowders with spherical nanoparticles were prepared by Cao et al. [22] who also disclosed the structural, optical, and photocatalytic studies. Even so, the main flaw of MnO2 is the low number of photo-generated electron-hole pairs and the rapid rate at which the pairs recombine, which reduces the photocatalytic effectiveness under both UV and visible light illuminations. The appropriate method has been modified to increase the photocatalytic efficacy of bare MnO_2 in order to fix this flaw. For instance, MnO_2 can be doped with metals, mixed with metal oxides, or used in combination with carbon-based materials to increase its photocatalytic efficiency. Dopant is the best option among these to enhance the pristine MnO_2's band gap energy and light absorption property. So, in order to enhance the photocatalytic efficacy, TiO_2 is added to MnO_2. In general, the size and shape of silver nanoparticles have a significant impact on their antibacterial, optical, thermal, and catalytic characteristics. TiO_2 can be added to MnO_2 to improve its capacity to absorb light while also reducing the rate at which electron-hole couples recombine. According to the author's best report, the research results are concentrated on the preparation of MnO_2 combined with TiO_2 using a straightforward sol-gel technique in order to obtain the improved photocatalytic degradation efficiency of TiO_2 doped MnO_2 structures under visible light illuminations.

2. Materials and methods

2.1. Preparation of pure and TiO_2 doped MnO_2 nanoparticles

Using TiO_2, $KMnO_4$, and $MnSO_4$, it was simple to create TiO_2 enriched MnO_2 nanoparticles.Raw elements are H_2O. $MnSO_4.H_2O$ (0.5 g) was first dissolved in 15 mL of water using a sonicator. The solution was then supplemented with $KMnO_4$ water dispersion (1 mg/mL) while being stirred magnetically. The MnO_2 precursor was combined with TiO_2, and the mixture was allowed to rapidly stirrer for 8 hours at 80 deg. C to produce gel-like form. The resulting gel was then cleaned by being washed repeatedly with distilled water and ethanol before being centrifuged at a speed of 3000 rpm. The acquired gel was then dried in a vacuum oven at 45 deg. C. The dark TiO_2 doped MnO_2 nano powders were finally collected. The same testing technique was used to obtain the pure MnO_2. All of the prepared examples were placed in an alumina crucible with a cover, heated for four hours at 400 °C, and then removed.

2.2. Characterization techniques

By using Cu-K as the radiation source (wavelength: 1.54056) and a scan rate of 0.50 s, X-ray powder diffraction (XRD, Bruker D8 Advance) was used to determine the structural characteristics of the produced samples. With the help of a JEOL JEM 2100F scanning electron microscope, microstructure research was carried out. (SEM). A Hitachi UV-365 spectrophotometer with an integrating sphere attachment and wavelength ranges of 300 to 700 nm was used to conduct the DRS observations. Raman spectra of the samples were recorded using a BRUKER IFS FT-IR Spectrometer at a resolution of 0.2 cm-1 to determine their fundamental vibration modes.

3. Results and discussion

3.1. Powder X-ray diffraction (XRD) analysis

The purity and phase nature of the samples was identified via XRD pattern and the resultant graph is shown in Figure 1. From the XRD profile clearly showing that both pure and MnO_2 doped TiO_2 samples are belongs to tetragonal crystal structure with space group of 12/m (87). The resulting miller indices are (200), (202), (220), (310), (211), (330), (301), (321), (521)

and (202) synchronized well with the standard value (JCPDS#44-0141). The TiO2 dopant does not impact the crystalline structure but improves the crystalline nature. The sharp and high intense peaks were detected for doped MnO_2 than pure MnO_2. Moreover, a slight shift in the lower angle side of the doped MnO_2 was observed. This may due to the advancing the crystalline nature. The found lattice parameters were just a bit higher than the bare MnO_2 (a = 9.802 and c = 2.8612) in terms of a and c. By measuring the crystalline size using Debye-Scherrer's equation, this effect was further discovered [24]. For MnO2 and MnO_2@TiO_2, the typical grain size was found to be 38 and 45 nm, respectively.

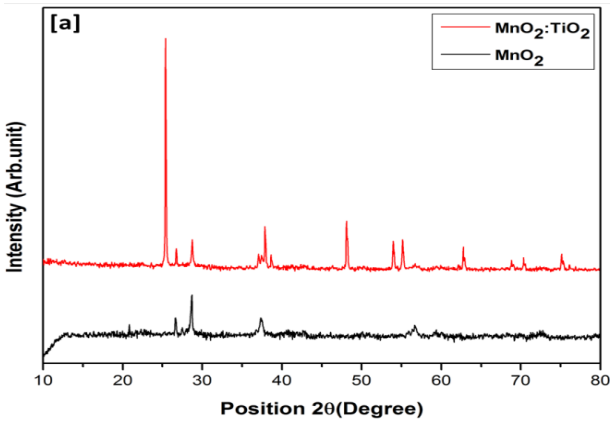

Fig. 1. Powder X-ray diffraction pattern of pure MnO_2 and doped TiO_2 samples.

3.2. FT-IR analysis

The FT-IR bands are captured between 4000 and 400 cm^{-1}. Manganese dioxide nanoparticles' FT-IR bands are displayed in Figure 2. When compared to bare MnO_2, these major peaks for MnO_2 doped TiO_2 are absent, demonstrating the existence of TiO_2. These major peaks were obtained at 3523, 2978, 1686, 1184, and 685 cm^{-1}. Both bare MnO_2 and doped MnO2 exhibit a wide band at 1686 cm^{-1}, which is consistent with the stretching mode of the -OH group. The H-O-H bending vibration of water found in the moisture absorbed from the environment is attributed to a band near 1686 cm^{-1}. O_2 ions could be the cause of bands around 1184 cm^{-1}. The peak at approximately 685 cm^{-1} is the typical Mn-O stretching absorption, indicating the creation of Mn-O bond in the prepared nanoparticles. The FT-IR spectra of altered iron oxide nanoparticles are displayed in Figure (2). On doping, the Ti-O peak's intensity also dropped. While a decline in intensity suggests that doping is low and has little effect on the Ti-O structure skeleton, a small shift in band indicates that doping in nanomaterials.

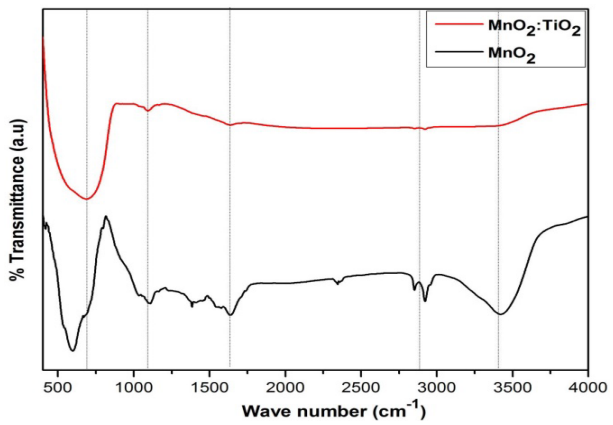

Fig. 2. FTIR spectrum of pure MnO_2 and doped TiO_2 nanomaterials.

According to Hook's law, which states that the vibration frequency is indirectly proportional to reduced mass in particular, as the condensed mass rises the vibrational frequency shifts to a deeper value, this reduction can be explained.

3.3. UV-Vis DRS analysis

In the area of photocatalyst, the band gap energy's absorption capacity and makeup are more crucial. As a result, the UV-DRS method was used to analyse these characteristics. The UV-Vis absorption spectra for both materials are displayed in Figure 3. The optical absorption maximum of bare MnO_2 and MnO_2 doped TiO_2 was determined to be 260 nm, showing that pure MnO_2 has a deeper absorption than doped MnO_2. These bands were also moved to a higher wavelength area of 450 nm. This might be because the samples' sizes varied. In addition, the surface plasmon resonance effect plays a significant part in lowering band gap energy. The Kubelka-Munk (K-M) model [27] was used to further corroborate the samples' reducing band gap. R is the proportion of reflectance, and F (R) = (1-R)2/2R gives the K-M model at any wavelength. The direct band gap energy [28] is used as the intercept number on a graph between [F (R) h]2 Vs h.

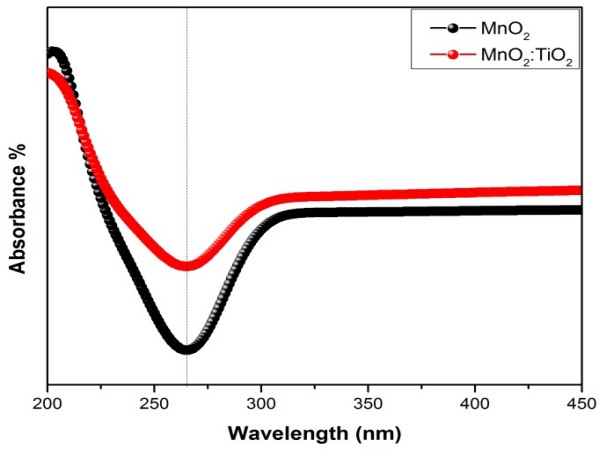

Fig. 3. UV-Vis DRS spectra of pure MnO_2 and doped TiO_2 samples

3.4. Raman analysis

Raman spectroscopy was used to further expose the structural information of the pure and TiO creation in MnO_2, and the resulting graph is depicted in Figure 4. For both bare MnO2 and doped MnO_2, two distinct maxima were found at 612 and 1607 cm^{-1}. The symmetric stretching vibration of Mn-O is linked to the vibration bands [25, 26]. The peak of doped MnO2 found near 400 is missing in pure MnO_2, which supports the formation of TiO in MnO_2, and there are vibration bands associated with TiO_2. As the TiO_2 content in the MnO_2 matrix grew, the peak intensity gradually increased. The size disparity between MnO2 and TiO doped MnO_2 may be the cause of this peak variation.. Results from XRD and SEM also provided an explanation for the variance in grain sizes of both pure and doped MnO2 [29].

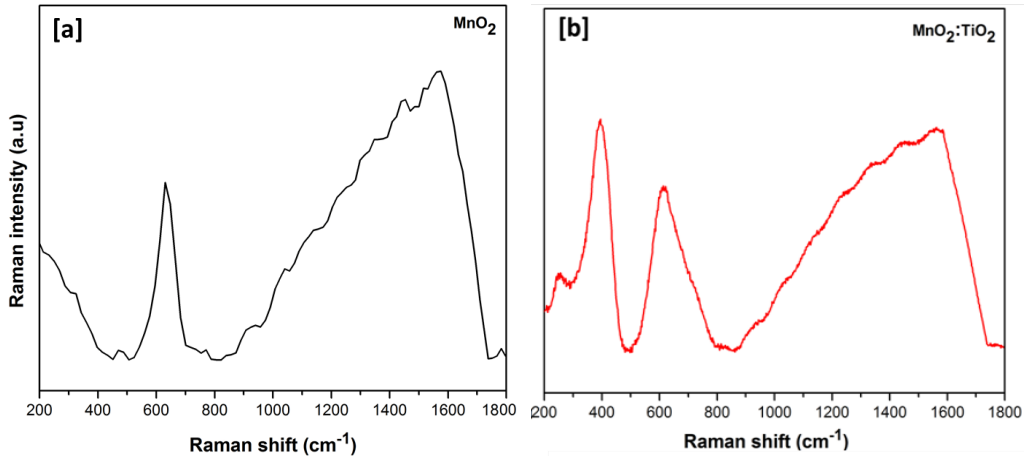

Fig. 4. Raman spectra of pure MnO_2 and doped TiO_2 samples

3.5. SEM and EDAX analysis

By using SEM images, the goods' detailed morphological and structural information was examined. The SEM pictures of pure and doped MnO_2 samples are shown in Figures 5(a&b), respectively.

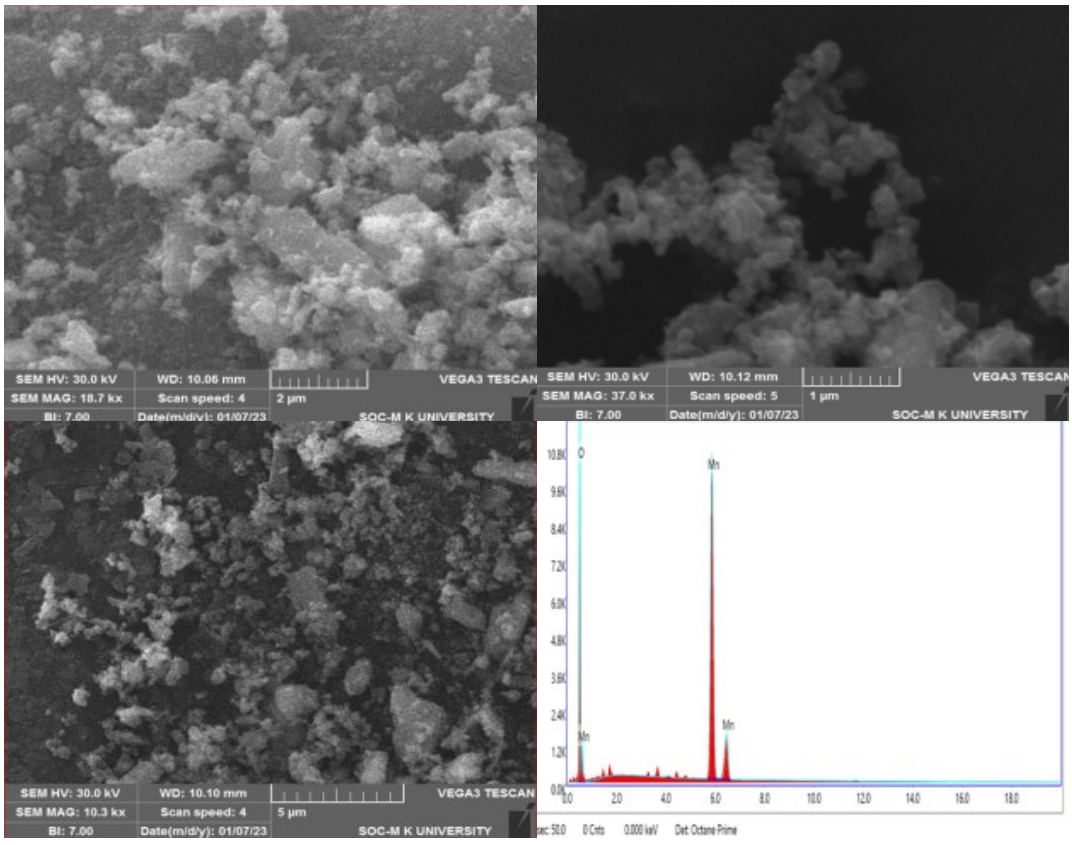

Fig. 5. (a). SEM images of pure MnO_2; and EDAX spectra of MnO_2.

Both examples demonstrate the presence of discernible spherical objects in ranges of uniform sizes. The Ti doped MnO2 samples exhibited less spherical agglomeration and increased dimension in the structures when compared to bare MnO_2. For the bare MnO_2 and doped samples, the typical particle size was determined to be 30 and 45 nm, respectively. SEM pictures were used

to further analyse the doped sample's structural data. It was evident that there are distinct fringes in the tetragonal MnO_2 phase's (310) plane of the lattice value d = 0.293 nm, which are in good agreement with the XRD findings EDAX spectra were used to determine the elements' makeup in addition. (Fig. 4). The primary components of Mn, O, and TiO_2 are revealed by the spectra of pure and doped MnO_2. Ti was successfully incorporated into the MnO_2 matrix as evidenced by the adding of TiO to the doped sample [30].

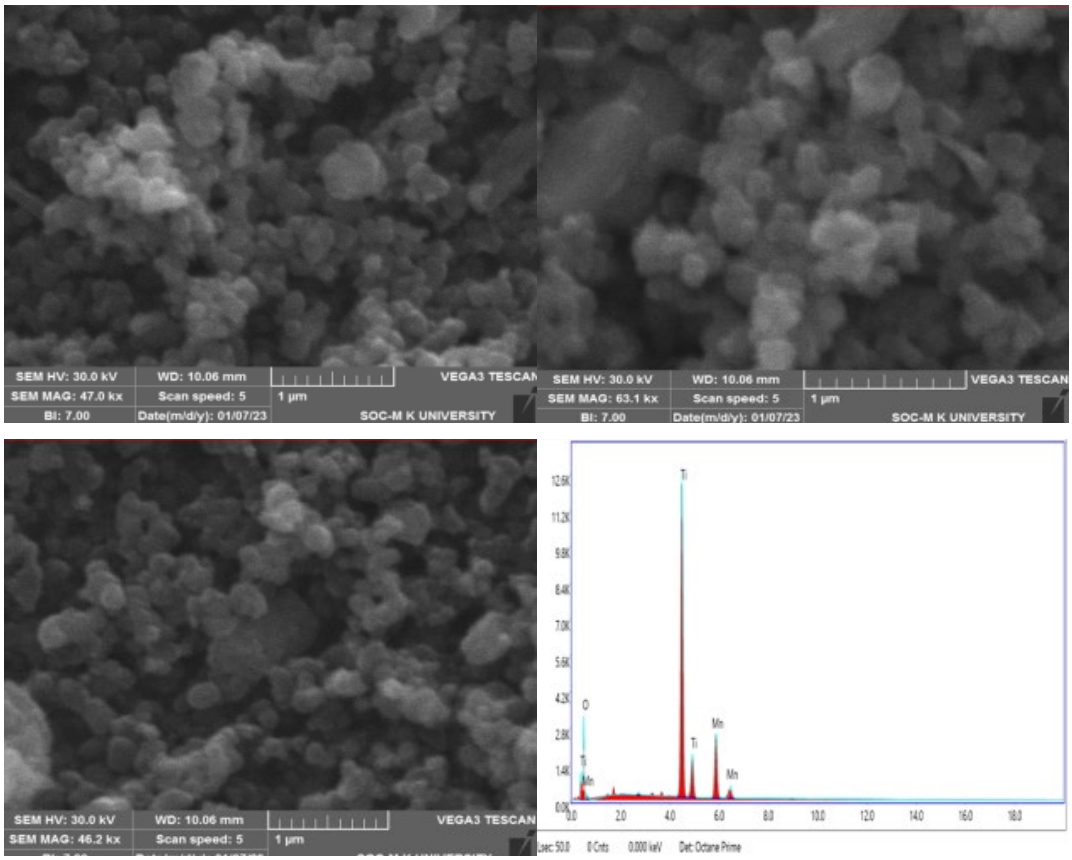

Fig. 2. (b). SEM images of MnO_2 doped TiO2 and EDAX spectra of MnO_2:TiO2.

3.6. Photocatalytic studies

To cause the photo-generated electron-hole pairs under visible light irradiation, time degradation and absorption skill are essential. Additionally, this is crucial for the photocatalytic decomposition process' dye deterioration. The ability to absorb light was originally discovered in order to understand the behaviour of photocatalytic activity. The UV-Vis absorption bands of MB dye using MnO2 and MnO_2@TiO_2 catalyst samples are shown in Figure 6(a&b) when illuminated by visible light. The highest MB absorption intensity was first noticed at 660 nm when there was no visible light present. The absorption intensity steadily decreased as the visible light illumination increased from 0 to 120 minutes. It was therefore obvious that the catalysts produced were more active in visible light. To corroborate the capability of the catalysts, the degradation efficiency of both dyes was further examined. The temporal degradation curve of MB dye using the catalysts is shown in Fig. 7(a & b) under visible light. The trial was conducted in a similar experimental setting. It was discovered that pure MnO2 has a high degradation efficiency of the MB dye (85%), and that as the amount of TiO_2 was progressively added, the efficiency of the MB dye was also linearly increased. The MnO_2 doped TiO_2 catalyst sample was found to reach the maximum efficiency of MB, which is 95%. The photocatalytic finding demonstrates unequivocally that doped MnO_2 catalyst demonstrated increased photocatalytic efficiency compared to bare MnO_2. Particularly, the MnO_2 doped TiO_2 catalyst under ideal conditions demonstrated superior

photocatalytic efficacy compared to other catalyst powders. This might be as a result of the doped samples' larger surface area, porous structure, and lower band gap energy when compared to bare MnO_2. The catalysts' pseudo-first-order kinetic equation was also found in order to understand more of the photocatalytic activity [31]. Different masses of the MnO2@TiO_2 catalyst were collected and exposed to the photocatalytic efficiency of MB dye. This produced advanced photocatalytic performance, and the degradation efficiency of the dyes was displayed in a bar diagram. The practical photocatalytic device and waste water treatment uses depend on reproducibility and long-term stability. Under the same experimental circumstances, all catalysts' stability tests were evaluated over five cycles, and Fig. 8's bar diagram displays the results. (a & b). Both dyes' photo-degradation effectiveness has not significantly decreased. Only 2.5% of the catalyst's original degradation effectiveness was lost after 7 cycles of operation. As a result, the catalyst that was collected is more resistant to the degradation of MB and phenol dyes when exposed to visible light. The improved process of the MnO2 doped TiO_2 catalyst under visible light is schematically depicted in Fig. 9 based on the photocatalytic test. Because more visible light is absorbed by the surface of the modified MnO_2, more photo-electrons are excited and become condensed, improving the photocatalytic behaviour of the material. As the Fermi level of MnO_2 doped TiO_2 lies between the conduction band and Fermi level of pure MnO_2, these excited electrons can be easily attracted to the TiO_2 nanoparticles. This leads to the formation of the Schottky junction at the MnO_2@TiO_2 interface, which improves the separation of photogenerated charge carriers and lowers their recombination rate [32]. Additionally, superoxide anion radicals are produced when excited electrons combine with O_2 molecules, whereas hydroxyl radicals are produced when excited holes interact with water. The photodegradation of MB pigment is brought on by these radicals. Additionally, the enormous surface area of MnO_2 doped TiO_2 could offer a sizable active site to capture the visible light on its surface, improving the prepared sample's ability to degrade.

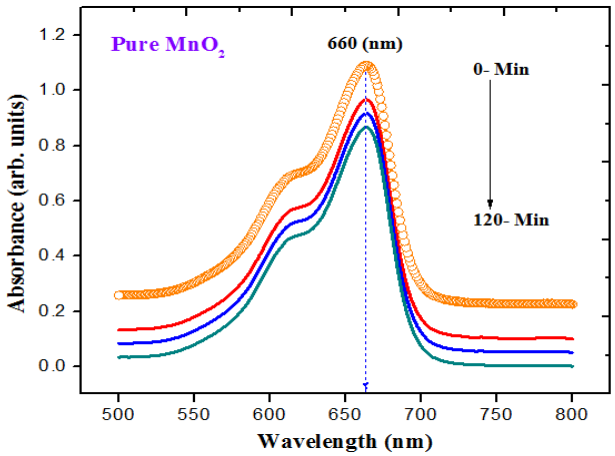

Fig. 7. (a) UV absorption spectra of MB using pure MnO_2 NPs.

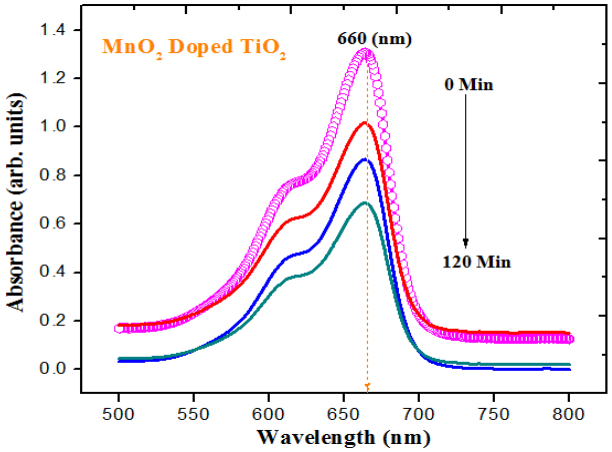

Fig. 7. (b) UV absorption spectra of MB using MnO_2 doped TiO_2 NPs.

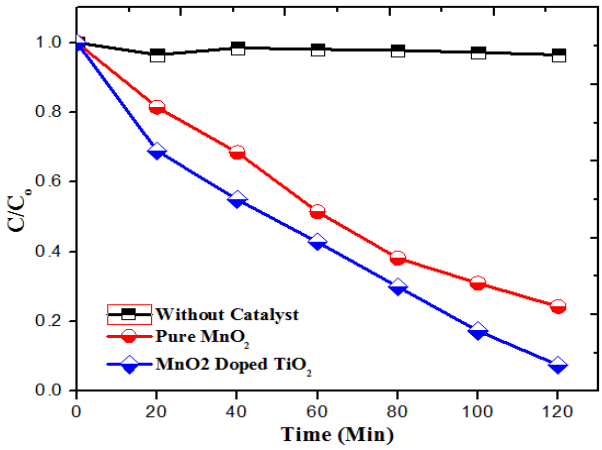

Fig. 8. (a) Temporal degradation profile of MB dye using pure MnO_2 under visible light irradiation.

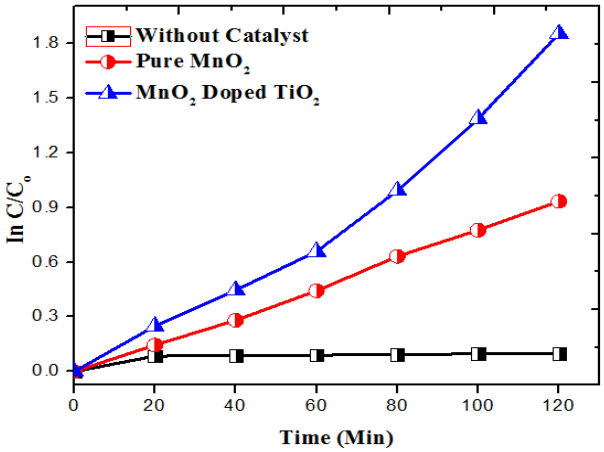

Fig. 8. (b) Temporal degradation curve of MB dye using TiO2 doped with MnO2 exposed to visible light.

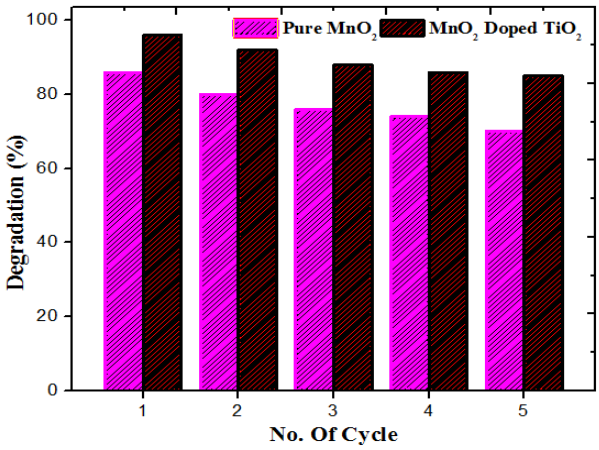

Fig. 9. Depicts, under visible light, the impact of the MnO2 doped TiO2 catalyst dosage on the degradation of the MB dye.

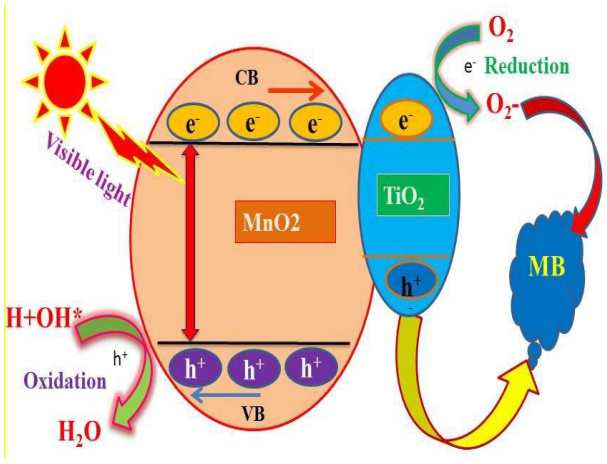

Fig. 10. MnO2 doped TiO2 catalysts' photocatalytic process when exposed to visible light.

4. Conclusions

Pure MnO_2 and TiO_2 incorporated MnO_2 nanoparticles were created using the straightforward sol-gel technique, and their scientific study included XRD, FTIR, UV, Raman, and SEM analysis to uncover their structural, morphological, and optical details. In order to investigate the photo-degradation efficiency of MB dye when exposed to visible light, a number of MnO_2 doped TiO_2 catalysts were made. The findings demonstrate that a doped MnO_2 catalyst operating at its peak demonstrated exceptional photocatalytic performance, including improved degradation efficiency and long-term stability. The band gap energy of the MnO_2 dopant TiO_2 that has been harvested has been decreased. As a result, it was determined that synthetic catalyst is a viable option for applications involving the degradation of environmental pollutants, such as waste water treatment.

References

[1] C.M. Magdalane, G.M.A. Priyadharsini, K. Kaviyarasu, A.I. Jothi, G.G. Simiyon, Surfaces and Interfaces, 25, 101296 (2021); https://doi.org/10.1016/j.surfin.2021.101296

[2] R. Renuka, K. Renuka Devi, M. Sivakami, T. Thilagavathi, R. Uthrakumar, K. Kaviyarasu,

Biocatal. Agric. Biotechnol. 24, 101567, (2020); https://doi.org/10.1016/j.bcab.2020.101567

[3] Sze-Mun Lam, Chew-Lin Lim, Jin-Chung Sin, Honghu Zeng, Hua Lin, Haixiang Li, Materials Letters, 305, 130818, (2021); https://doi.org/10.1016/j.matlet.2021.130818

[4] S. Logambal, C. Maheswari, S. Chandrasekar, T. Thilagavathi, C. Inmozhi, S. Panimalar, F.A. Bassyouni, R. Uthrakumar, Mohamed Ragab Abdel Gawwad, Reem M. Aljowaie, Dunia A. Al Farraj, K. Kanimozhi, J. King Saud Uni. - Sci., 34, 101910, (2022); https://doi.org/10.1016/j.jksus.2022.101910

[5] Amal George, D. Magimai Antoni Raj, X. Venci, A. Dhayal Raj, A. Albert Irudayaraj, R.L. Josephine, S. John Sundaram, Amal A. Al-Mohaimeed, Dunia A. Al Farraj, Tse-Wei Chen, K. Kaviyarasu, Environmental Research, 203, 111880 (2022); https://doi.org/10.1016/j.envres.2021.111880

[6] Muhammad Aadil, Majid Mahmood, Muhammad Farooq Warsi, Ibrahim A. Alsafari, Sonia Zulfiqar, Muhammad Shahid, FlatChem, 30, 100316, (2021); https://doi.org/10.1016/j.flatc.2021.100316

[7] S. Panimalar, S. Logambal, R. Thambidurai, C. Inmozhi, R. Uthrakumar, Azhaguchamy Muthukumaran, Rabab Ahmed Rasheed, Mansour K. Gatasheh, A. Raja, J. Kennedy, K. Kaviyarasu, Environmental Research, 205, 112560, (2022); https://doi.org/10.1016/j.envres.2021.112560

[8] Lian Wang, Hong He, Changbin Zhang, Li Sun, Sijin Liu, Shaoxin Wang, J. of Environ. Sci., 41, 112, (2016); https://doi.org/10.1016/j.jes.2015.04.026

[9] S. Panimalar, M. Subash, M. Chandrasekar, R. Uthrakumar, C. Inmozhi, Wedad A. Al-Onazi, Amal M. Al-Mohaimeed, Tse-Wei Chen, J. Kennedy, M. Maaza, K. Kaviyarasu, Chemosphere, 293, 133646, (2022); https://doi.org/10.1016/j.chemosphere.2022.133646

[10] N. Geetha, S. Sivaranjani, A. Ayeshamariam, M. Siva Bharathy, S. Nivetha, K. Kaviyarasu, M. Jayachandran, Journal of Advanced Microscopy Research 13 (1), 12, (2018); https://doi.org/10.1166/jamr.2018.1352

[11] Shenqiang Wang, Hua Zheng, Li Zhou, Fang Cheng, Zhao Liu, Hepeng Zhang, Qiuyu Zhang, Biomaterials, 260, 120314, (2020); https://doi.org/10.1016/j.biomaterials.2020.120314

[12] N.M.I. Alhaji, D. Nathiya, K. Kaviyarasu, M. Meshram, A. Ayeshamariam, Surfaces and Interfaces 17, 100375, (2019); https://doi.org/10.1016/j.surfin.2019.100375

[13] G. Nayanmoni, K.B. Punuri Jayase, M. Chandan, B. Utpal, Material science and Engineering, 46, 463, (2015); https://doi.org/10.1016/j.msec.2014.10.069

[14] L. Shangpeng, M. Jianwei, S Wang, C. Shaojuan, W. Bin, Jiwei Li, Materials Letters, 255, 126570, (2019); https://doi.org/10.1016/j.matlet.2019.126570

[15] W. Wu, ZW. Taekyung, C. Jiang, Sci-Technol. Adv. Mater 16, 1, (2015); https://doi.org/10.1088/1468-6996/16/2/023501

[16] A. George, A. Dhayal Raj, A. Albert Irudayaraj, R.L. Josephine, X. Venci, S. John Sundaram, R. Rajakrishnan, P. Kuppusamy, K. Kaviyarasu, Environmental Research, 211, 112970, (2022); https://doi.org/10.1016/j.envres.2022.112970

[17] Surya Narayana Maddila, Suresh Maddila, Sandeep V.H.S. Bhaskaruni, Nagaraju Kerru, Sreekantha B. Jonnalagadda, Inorganic Chemistry Communications, 112, 107706, (2020); https://doi.org/10.1016/j.inoche.2019.107706

[18] V. Perumal, C. Inmozhi, R. Uthrakiumar, R. Robert, M. Chandrasekar, S. Beermohamed, shehla Honely, A. Raja, Fahd. A .Al-Mekhlafi, K. Kaviyarasu, Environmental Research, 209, 112821, (2022); https://doi.org/10.1016/j.envres.2022.112821

[19] R.D. Shannon, Acta crystallogr. A32, 751, (1976); https://doi.org/10.1107/S0567739476001551

[20] S. Panimalar, R. Uthrakumar, E. Tamil Selvi, P. Gomathy, C. Inmozhi, K. Kaviyarasu, J. Kennedy, Surfaces and Interfaces 20, 100512, (2020); https://doi.org/10.1016/j.surfin.2020.100512

[21] X. Dong, X. Wang, J. Wang, H. Song, X.Li, L. Wang, M.B. Chanpark, C.M. Li, P. Chen, Carbon, 50, 4865, (2012); https://doi.org/10.1016/j.carbon.2012.06.014

[22] N. Manjula, K. Kaviyarasu, A. Ayeshamariam, G. Selvan, A. Diallo, G. Ramalingam, S.B. Mohamed, D. Letsholathebe, M. Jayachandran, Journal of Nanoelectronics and Optoelectronics, 13 (10), 1543, (2018); https://doi.org/10.1166/jno.2018.2384

[23] M.V. Arularasu, M. Anbarasu, S. Poovaragan, R. Sundaram, K. Kanimozhi, C. Maria Magdalane, K. Kaviyarasu, F.T. Thema, Douglas Letsholathebe, Genene T. Mola, M. Maaza, Journal of nanoscience and nanotechnology 18 (5), 3511, (2018); https://doi.org/10.1166/jnn.2018.14658

[24] Danni Ding, Yu Zhou, Taohong He, Shaopeng Rong, Chemical Engineering Journal, 431, 133737, (2022); https://doi.org/10.1016/j.cej.2021.133737

[25] S. Panimalar, M. Chandrasekar. S. Logambal, R. Uthrakumar, C. Inmozhi, Materials Today: Proceedings, 56, 3394, (2022); https://doi.org/10.1016/j.matpr.2021.10.335

[26] Cheng Xie, Lei Xu, Yi Xia, Ruiqi Gang, Qianjun Ye, Sivasankar Koppala, Microporous and Mesoporous Materials, 334, 111788, (2022); https://doi.org/10.1016/j.micromeso.2022.111788

[27] M. Chandrasekar, M. Subash, V. Perumal, S. Panimalar, S. Aravindan, R. Uthrakumar, C. Inmozhi, Abdulgalim B. Isaev, Sudhakar Muniyasamy, A. Raja, K. Kaviyarasu, Separation and Purification Technology, 294, 121189, (2022); https://doi.org/10.1016/j.seppur.2022.121189

[28] Manita Khatri, Aakash Gupta, Kabita Gyawali, Anup Adhikari, Agni Raj, Koirala, Niranjan Parajuli, Chemical Data Collections, 39, 100854, (2022); https://doi.org/10.1016/j.cdc.2022.100854

[29] V. Perumal, A. Sabarinathan, M. Chandrasekar, M. Subash, C. Inmozhi, R. Uthrakumar, Abdulgalim B. Isaev, A. Raja, Mohamed S. Elshikh, Saeedah Musaed Almutairi, K. Kaviyarasu, Fuel, 324, 124599, (2022); https://doi.org/10.1016/j.fuel.2022.124599

[30] Weiwei Yu, Tiangui Liu, Shiyi Cao, Chen Wang, Chuansheng Chen, Journal of Solid State Chemistry, 239, 131, (2016); https://doi.org/10.1016/j.jssc.2016.04.027

[31] M. Rahmat, H.N. Bhatti, A. Rehman, H. Chaudhry, M. Yameen, M. Iqbal, S.H. Al-Mijalli, N. Alwadai, M.Fatima, M. Abbas, Arabian Journal of Chemistry, 14, 103415, (2021); https://doi.org/10.1016/j.arabjc.2021.103415

[32] Sze-Mun Lam, Chew-Lin Lim, Jin-Chung Sin, Honghu Zeng, Hua Lin, Haixiang Li, Materials Letters, 305, 130818, (2021); https://doi.org/10.1016/j.matlet.2021.130818